Search for Charged Excited Leptons in e$^+$e$^-$ Collisions at $\sqrt{s}$ = 183-209 GeV

The OPAL Collaboration

Abstract

A search for charged excited leptons decaying into a lepton and a photon has been performed using approximately 680 pb^{-1} of e$^+$e$^-$ collision data collected by the OPAL detector at LEP at centre-of-mass energies between 183 GeV and 209 GeV. No evidence for their existence was found. Upper limits on the product of the cross-section and the branching fraction are inferred. Using results from the search for singly produced excited leptons, upper limits on the ratio of the excited lepton coupling constant to the compositeness scale are calculated. From pair production searches, 95% confidence level lower limits on the masses of excited electrons, muons and taus are determined to be 103.2 GeV.

The OPAL Collaboration

G. Abbiendi[2], C. Ainsley[5], P.F. Åkesson[3], G. Alexander[22], J. Allison[16], P. Amaral[9],
G. Anagnostou[1], K.J. Anderson[9], S. Arcelli[2], S. Asai[23], D. Axen[27], G. Azuelos[18,a], I. Bailey[26],
E. Barberio[8], R.J. Barlow[16], R.J. Batley[5], P. Bechtle[25], T. Behnke[25], K.W. Bell[20], P.J. Bell[1],
G. Bella[22], A. Bellerive[6], G. Benelli[4], S. Bethke[32], O. Biebel[32], I.J. Bloodworth[1], O. Boeriu[10],
P. Bock[11], D. Bonacorsi[2], M. Boutemeur[31], S. Braibant[8], L. Brigliadori[2], R.M. Brown[20],
K. Buesser[25], H.J. Burckhart[8], J. Cammin[3], S. Campana[4], R.K. Carnegie[6], B. Caron[28],
A.A. Carter[13], J.R. Carter[5], C.Y. Chang[17], D.G. Charlton[1,b], I. Cohen[22], A. Csilling[8,g],
M. Cuffiani[2], S. Dado[21], G.M. Dallavalle[2], S. Dallison[16], A. De Roeck[8], E.A. De Wolf[8],
K. Desch[25], M. Donkers[6], J. Dubbert[31], E. Duchovni[24], G. Duckeck[31], I.P. Duerdoth[16],
E. Elfgren[18], E. Etzion[22], F. Fabbri[2], L. Feld[10], P. Ferrari[12], F. Fiedler[31], I. Fleck[10], M. Ford[5],
A. Frey[8], A. Fürtjes[8], P. Gagnon[12], J.W. Gary[4], G. Gaycken[25], C. Geich-Gimbel[3],
G. Giacomelli[2], P. Giacomelli[2], M. Giunta[4], J. Goldberg[21], E. Gross[24], J. Grunhaus[22],
M. Gruwé[8], P.O. Günther[3], A. Gupta[9], C. Hajdu[29], M. Hamann[25], G.G. Hanson[4], K. Harder[25],
A. Harel[21], M. Harin-Dirac[4], M. Hauschild[8], J. Hauschildt[25], C.M. Hawkes[1], R. Hawkings[8],
R.J. Hemingway[6], C. Hensel[25], G. Herten[10], R.D. Heuer[25], J.C. Hill[5], K. Hoffman[9], R.J. Homer[1],
D. Horváth[29,c], R. Howard[27], P. Hüntemeyer[25], P. Igo-Kemenes[11], K. Ishii[23], H. Jeremie[18],
P. Jovanovic[1], T.R. Junk[6], N. Kanaya[26], J. Kanzaki[23], G. Karapetian[18], D. Karlen[6],
V. Kartvelishvili[16], K. Kawagoe[23], T. Kawamoto[23], R.K. Keeler[26], R.G. Kellogg[17],
B.W. Kennedy[20], D.H. Kim[19], K. Klein[11], A. Klier[24], S. Kluth[32], T. Kobayashi[23], M. Kobel[3],
T.P. Kokott[3], S. Komamiya[23], L. Kormos[26], R.V. Kowalewski[26], T. Krämer[25], T. Kress[4],
P. Krieger[6,l], J. von Krogh[11], D. Krop[12], M. Kupper[24], P. Kyberd[13], G.D. Lafferty[16],
H. Landsman[21], D. Lanske[14], J.G. Layter[4], A. Leins[31], D. Lellouch[24], J. Letts[12], L. Levinson[24],
J. Lillich[10], S.L. Lloyd[13], F.K. Loebinger[16], J. Lu[27], J. Ludwig[10], A. Macpherson[28,i], W. Mader[3],
S. Marcellini[2], T.E. Marchant[16], A.J. Martin[13], J.P. Martin[18], G. Masetti[2], T. Mashimo[23],
P. Mättig[m], W.J. McDonald[28], J. McKenna[27], T.J. McMahon[1], R.A. McPherson[26], F. Meijers[8],
P. Mendez-Lorenzo[31], W. Menges[25], F.S. Merritt[9], H. Mes[6,a], A. Michelini[2], S. Mihara[23],
G. Mikenberg[24], D.J. Miller[15], S. Moed[21], W. Mohr[10], T. Mori[23], A. Mutter[10], K. Nagai[13],
I. Nakamura[23], H.A. Neal[33], R. Nisius[8], S.W. O'Neale[1], A. Oh[8], A. Okpara[11], M.J. Oreglia[9],
S. Orito[23], C. Pahl[32], G. Pásztor[8,g], J.R. Pater[16], G.N. Patrick[20], J.E. Pilcher[9], J. Pinfold[28],
D.E. Plane[8], B. Poli[2], J. Polok[8], O. Pooth[14], M. Przybycień[8,j], A. Quadt[3], K. Rabbertz[8],
C. Rembser[8], P. Renkel[24], H. Rick[4], J.M. Roney[26], S. Rosati[3], Y. Rozen[21], K. Runge[10],
D.R. Rust[12], K. Sachs[6], T. Saeki[23], O. Sahr[31], E.K.G. Sarkisyan[8,j], A.D. Schaile[31], O. Schaile[31],
P. Scharff-Hansen[8], J. Schieck[32], T. Schoerner-Sadenius[8], M. Schröder[8], M. Schumacher[3],
C. Schwick[8], W.G. Scott[20], R. Seuster[14,f], T.G. Shears[8,h], B.C. Shen[4],
C.H. Shepherd-Themistocleous[5], P. Sherwood[15], G. Siroli[2], A. Skuja[17], A.M. Smith[8], R. Sobie[26],
S. Söldner-Rembold[10,d], S. Spagnolo[20], F. Spano[9], A. Stahl[3], K. Stephens[16], D. Strom[19],
R. Ströhmer[31], S. Tarem[21], M. Tasevsky[8], R.J. Taylor[15], R. Teuscher[9], M.A. Thomson[5],
E. Torrence[19], D. Toya[23], P. Tran[4], T. Trefzger[31], A. Tricoli[2], I. Trigger[8], Z. Trócsányi[30,e],
E. Tsur[22], M.F. Turner-Watson[1], I. Ueda[23], B. Ujvári[30,e], B. Vachon[26], C.F. Vollmer[31],
P. Vannerem[10], M. Verzocchi[17], H. Voss[8], J. Vossebeld[8], D. Waller[6], C.P. Ward[5], D.R. Ward[5],
P.M. Watkins[1], A.T. Watson[1], N.K. Watson[1], P.S. Wells[8], T. Wengler[8], N. Wermes[3],
D. Wetterling[11] G.W. Wilson[16,k], J.A. Wilson[1], G. Wolf[24], T.R. Wyatt[16], S. Yamashita[23],
V. Zacek[18], D. Zer-Zion[4], L. Zivkovic[24]

[1]School of Physics and Astronomy, University of Birmingham, Birmingham B15 2TT, UK
[2]Dipartimento di Fisica dell' Università di Bologna and INFN, I-40126 Bologna, Italy
[3]Physikalisches Institut, Universität Bonn, D-53115 Bonn, Germany

[4]Department of Physics, University of California, Riverside CA 92521, USA

[5]Cavendish Laboratory, Cambridge CB3 0HE, UK

[6]Ottawa-Carleton Institute for Physics, Department of Physics, Carleton University, Ottawa, Ontario K1S 5B6, Canada

[8]CERN, European Organisation for Nuclear Research, CH-1211 Geneva 23, Switzerland

[9]Enrico Fermi Institute and Department of Physics, University of Chicago, Chicago IL 60637, USA

[10]Fakultät für Physik, Albert-Ludwigs-Universität Freiburg, D-79104 Freiburg, Germany

[11]Physikalisches Institut, Universität Heidelberg, D-69120 Heidelberg, Germany

[12]Indiana University, Department of Physics, Swain Hall West 117, Bloomington IN 47405, USA

[13]Queen Mary and Westfield College, University of London, London E1 4NS, UK

[14]Technische Hochschule Aachen, III Physikalisches Institut, Sommerfeldstrasse 26-28, D-52056 Aachen, Germany

[15]University College London, London WC1E 6BT, UK

[16]Department of Physics, Schuster Laboratory, The University, Manchester M13 9PL, UK

[17]Department of Physics, University of Maryland, College Park, MD 20742, USA

[18]Laboratoire de Physique Nucléaire, Université de Montréal, Montréal, Québec H3C 3J7, Canada

[19]University of Oregon, Department of Physics, Eugene OR 97403, USA

[20]CLRC Rutherford Appleton Laboratory, Chilton, Didcot, Oxfordshire OX11 0QX, UK

[21]Department of Physics, Technion-Israel Institute of Technology, Haifa 32000, Israel

[22]Department of Physics and Astronomy, Tel Aviv University, Tel Aviv 69978, Israel

[23]International Centre for Elementary Particle Physics and Department of Physics, University of Tokyo, Tokyo 113-0033, and Kobe University, Kobe 657-8501, Japan

[24]Particle Physics Department, Weizmann Institute of Science, Rehovot 76100, Israel

[25]Universität Hamburg/DESY, Institut für Experimentalphysik, Notkestrasse 85, D-22607 Hamburg, Germany

[26]University of Victoria, Department of Physics, P O Box 3055, Victoria BC V8W 3P6, Canada

[27]University of British Columbia, Department of Physics, Vancouver BC V6T 1Z1, Canada

[28]University of Alberta, Department of Physics, Edmonton AB T6G 2J1, Canada

[29]Research Institute for Particle and Nuclear Physics, H-1525 Budapest, P O Box 49, Hungary

[30]Institute of Nuclear Research, H-4001 Debrecen, P O Box 51, Hungary

[31]Ludwig-Maximilians-Universität München, Sektion Physik, Am Coulombwall 1, D-85748 Garching, Germany

[32]Max-Planck-Institute für Physik, Föhringer Ring 6, D-80805 München, Germany

[33]Yale University, Department of Physics, New Haven, CT 06520, USA

[a] and at TRIUMF, Vancouver, Canada V6T 2A3

[b] and Royal Society University Research Fellow

[c] and Institute of Nuclear Research, Debrecen, Hungary

[d] and Heisenberg Fellow

[e] and Department of Experimental Physics, Lajos Kossuth University, Debrecen, Hungary

[f] and MPI München

[g] and Research Institute for Particle and Nuclear Physics, Budapest, Hungary

[h] now at University of Liverpool, Dept of Physics, Liverpool L69 3BX, UK

[i] and CERN, EP Div, 1211 Geneva 23

[j] and Universitaire Instelling Antwerpen, Physics Department, B-2610 Antwerpen, Belgium

[k] now at University of Kansas, Dept of Physics and Astronomy, Lawrence, KS 66045, USA

[l] now at University of Toronto, Dept of Physics, Toronto, Canada

[m] current address Bergische Universität, Wuppertal, Germany

1 Introduction

Models in which fermions have substructure attempt to explain, among other things, the well-ordered pattern of fermion generations observed in nature. The existence of excited states of the Standard Model fermions would be a natural consequence of fermion compositeness. Excited leptons could be produced in e^+e^- collisions and are expected to decay via the emission of a gauge boson (γ, Z^0 or $W^\pm$) [1].

This paper presents results from a search for excited electrons (e^*), muons (μ^*) and tau leptons (τ^*) decaying electromagnetically, using data collected by the OPAL experiment at LEP. Results presented in this paper are obtained using a larger data sample, as well as a significantly improved analysis, compared to our previous publications [2]. Searches for excited leptons have also been performed by other LEP collaborations [3] and by the HERA experiments in electron-proton collisions [4].

At LEP, excited leptons could be produced in pairs or in association with a Standard Model lepton. Both single and pair production of excited leptons proceed through s-channel photon and Z^0 diagrams. In addition, t-channel photon and Z^0 exchange diagrams contribute to the single and pair production of excited electrons. The t-channel contribution, although expected to be negligible for pair production, causes excited electrons to be singly produced predominantly in the forward region with the recoiling electron outside the detector acceptance. Thus, in addition to final states containing two leptons and one or two photons ($\ell\ell\gamma$, $\ell\ell\gamma\gamma$), a separate search for the single production of excited electrons with an undetected electron ($e\gamma$) is also performed.

The results presented in this paper are interpreted in the context of the framework described in [5,6]. In this phenomenological model, the interaction between excited leptons and a gauge boson ($\ell^*\ell^*V$), which largely determines the cross-section for pair production of excited leptons, is vector-like. The single production cross-section and branching fractions of excited leptons are determined by the strength of the $\ell\ell^*V$ coupling. This interaction can be described by the following SU(2)×U(1) gauge invariant effective Lagrangian [5,6]

$$\mathcal{L}_{\ell\ell^*V} = \frac{1}{2\Lambda} \bar{\ell}^* \sigma^{\mu\nu} \left[gf\frac{\boldsymbol{\tau}}{2}\mathbf{W}_{\mu\nu} + g'f'\frac{Y}{2}B_{\mu\nu} \right] \ell_{\mathrm{L}} + \text{hermitian conjugate,}$$

where $\sigma^{\mu\nu}$ is the covariant bilinear tensor, $\boldsymbol{\tau}$ denotes the Pauli matrices, Y is the weak hypercharge, $\mathbf{W}_{\mu\nu}$ and $B_{\mu\nu}$ represent the Standard Model gauge field tensors and the couplings g, g' are the SU(2) and U(1) coupling constants of the Standard Model. The compositeness scale is set by the parameter Λ which has units of energy. Finally, the strength of the $\ell\ell^*V$ coupling is governed by the constants f and f'. These constants can be interpreted as weight factors associated with the different gauge groups. The values of f and f' dictate the relative branching fractions of excited leptons to each gauge boson. The branching fraction of electromagnetically decaying excited charged leptons is significant for most values of f and f' except in the case where $f = -f'$ which entirely forbids this particular decay. As a result of the clean characteristic signatures expected, the photon decay constitutes one of the most sensitive channels for the search for excited leptons, even for values of f and f' for which other decay modes dominate. To reduce the number of free parameters it is customary to assume either a relation between f and f' or set one coupling to zero. For easy comparison with previously published results, limits calculated in this paper correspond to the coupling choice $f = f'$. This assignment is a natural choice which forbids excited neutrinos from decaying electromagnetically. For this particular coupling choice, the electromagnetic branching fraction of charged excited leptons drops smoothly from 100% for masses below the Z^0 and $W^\pm$ mass thresholds to about 30% for masses in excess of 200 GeV.

$\sqrt{s}$ bin range (GeV)	$< \sqrt{s} >$ (GeV)	$\mathcal{L}$ (pb^{-1})
178.00 - 186.00	182.7	63.8
186.00 - 190.40	188.6	183.2
190.40 - 194.00	191.6	29.3
194.00 - 198.00	195.5	76.5
198.00 - 201.00	199.5	76.9
201.00 - 203.75	201.9	44.5
203.75 - 204.25	203.9	1.5
204.25 - 204.75	204.6	9.7
204.75 - 205.25	205.1	60.0
205.25 - 205.75	205.4	3.6
205.75 - 206.25	206.1	14.3
206.25 - 206.75	206.5	107.3
206.75 - 207.25	206.9	5.7
207.25 - 207.75	207.5	0.5
207.75 - 208.25	208.0	7.2
> 208.25	208.3	0.5
		684.4

Table 1: The luminosity weighted mean centre-of-mass energy and integrated luminosity of each energy bin.

2 Data and Simulated Event Samples

The data analysed were collected by the OPAL detector [7] at centre-of-mass energies ranging from 183 GeV to 209 GeV during the LEP runs in the years 1997 to 2000. The search for excited leptons is based on a total of 684.4 pb^{-1} of data for which all relevant detector components were fully operational. For the purpose of accurately interpreting the results in terms of limits on excited lepton masses and couplings, the data are divided into 16 centre-of-mass energy bins analysed separately. The energy range, luminosity weighted mean centre-of-mass energy and integrated luminosity of each bin are summarised in Table 1. The uncertainty on the measured beam energy is approximately 25 MeV [8] and is correlated between centre-of-mass energy bins. In addition to the high energy data, approximately 10 pb^{-1} of calibration data collected in 1997-2000 at a centre-of-mass energy near the Z^0 mass were used to study the detector response.

Distributions of kinematic variables and selection efficiencies for excited leptons were modelled using samples of simulated events obtained using the EXOTIC [9] Monte Carlo event generator. The matrix elements [5,10] implemented in EXOTIC include all the spin correlations in the production and decay of excited leptons.

The Standard Model processes at different centre-of-mass energies were simulated using a variety of Monte Carlo event generators. Bhabha events were simulated using the BH-WIDE [11] and TEEGG [12] generators, muon and tau pair events using both KORALZ [13] and KK2F [14], $e^+e^- \rightarrow q\bar{q}(\gamma)$ events using PYTHIA [15] and KK2F, four fermion processes using KORALW [16] and grc4f [17], di-photon production using RADCOR [18], and two-photon events ($e^+e^- \rightarrow e^+e^-\gamma\gamma \rightarrow e^+e^- f\bar{f}$) using VERMASEREN [19], PHOJET [20] and HERWIG [21]. Each of the simulated event samples was processed through the OPAL detector simulation program [22] and analysed in the same way as data.

3   Event Selection and Kinematic Fits

Events are reconstructed from tracks and energy clusters defined by requirements similar to those described in [23]. The background from multihadronic events is substantially reduced by requiring at least one but no more than six tracks in an event. Furthermore, the ratio of the number of good tracks, as defined in [23], to the total number of tracks reconstructed in the detector must be greater than 0.2 in order to reduce background from beam-gas and beam-wall collisions. Cosmic ray events are suppressed using information from the time-of-flight counters and the central tracking chamber [24].

Tracks and energy clusters in an event are grouped into jets using a cone algorithm [25] with a cone half-angle of 0.25 radians and minimum jet energy of 2.5 GeV. The parameters defining a jet were chosen to maximise the signal efficiency over the broadest possible range of excited lepton masses and centre-of-mass energies. Events are required to contain between two and four jets. Jets are classified as leptons or photons using the criteria described below applied in the same order as given in the text.

Photon candidates must have a minimum energy deposited in the electromagnetic calorimeter equivalent to 5% of the beam energy. A photon jet must either contain no tracks or be identified as a photon conversion using a neural network technique [26]. Jets in which the most energetic track has a neural network output greater than 0.9 and the energy deposited in the hadronic calorimeter is less than 10% of the beam energy are defined to be photon conversions. All photon candidates must lie within $|\cos\theta| < 0.9$ to avoid poorly modelled regions of the detector [1]. The energy and direction of each photon candidate are determined from the energy and position of the energy cluster in the electromagnetic calorimeter.

Muon candidates are jets containing exactly one track with associated hits in the muon detectors or hits in the hadronic calorimeter consistent with the particle being a muon [27]. Muons, unlike electrons and photons, do not shower while traversing additional material present in the forward region of the detector. Muon candidates are thus allowed to lie within a larger angular acceptance of $|\cos\theta| < 0.95$. The direction of each muon candidate is given by the polar and azimuthal angles of the track and the momentum is calculated from the track curvature and polar angle.

A jet is identified as an electron if it contains exactly one track satisfying one of the following two requirements: the ratio of the electromagnetic energy to the track momentum (E/p) lies between 0.8 and 1.4 or the track has an output greater than 0.9 from a neural network developed to identify electrons [26]. Electron candidates are also required to lie within $|\cos\theta| < 0.9$ to avoid poorly modelled regions of the detector. The energy of each electron candidate is taken to be the energy deposited in the electromagnetic calorimeter while the direction is given by the polar and azimuthal angles of the track.

Finally, unidentified jets containing at least one track and lying within $|\cos\theta| < 0.95$ are considered to be tau candidates. Jets in the region $0.90 < |\cos\theta| < 0.95$ which would satisfy the electron or photon requirements are discarded from the sample of tau candidates. Jets identified as tau candidates are mostly hadronically decaying taus. Tau leptons decaying leptonically are tagged as electrons or muons by the criteria described above. The polar and azimuthal angles of tau candidates are given by the axis of the jet, corrected for double-counting of tracks and energy clusters [28].

The different selections used to identify the final states of interest are described in the following sections and the results are summarised in Table 2.

---

[1]The OPAL coordinate system is defined to be right-handed, with the z-axis pointing along the electron beam direction and the x-axis pointing toward the centre of the LEP ring. Thus the polar angle θ used in this paper refers to the angle with respect to the electron beam direction and the azimuthal angle ϕ, the angle measured with respect to the x-axis.

3.1 Selection of $\ell\ell\gamma\gamma$ Final States

Events containing two lepton candidates of the same flavour and two identified photons are considered as candidate events for the pair production of excited leptons. In addition, events containing two leptons of different flavours and two photons are considered as excited tau candidates. In order to reduce the background from Standard Model processes, additional selection criteria are applied to the different types of candidate events.

The quantity R_{vis} is defined to be the sum of the energy of the particles considered for a given event final state, divided by the centre-of-mass energy. This quantity is required to exceed 0.8 for ee$\gamma\gamma$ and $\mu\mu\gamma\gamma$ candidates and 0.4 for $\tau\tau\gamma\gamma$ candidates. This criterion reduces the background from two-photon events. It also decreases the contamination from q$\bar{\mathrm{q}}$ events in the $\tau\tau\gamma\gamma$ sample. Figure 1(a-c) shows the R_{vis} distributions obtained using the entire data set for each type of candidate event. The observed discrepancy at small values of R_{vis} in the $\tau\tau\gamma\gamma$ sample corresponds to a region where the background is dominated by two-photon events and does not affect the analysis as the events of interest lie in a region of R_{vis} that is well modelled. A similar mis-modelling is present in distributions of $\ell\ell\gamma$ and eγ candidate events.

The remaining background in the ee$\gamma\gamma$ and $\mu\mu\gamma\gamma$ samples comes almost entirely from e$^+$e$^-$ and $\mu^+\mu^-$ events with additional photons. The background in the $\tau\tau\gamma\gamma$ sample consists mostly of $\tau^+\tau^-$ events with more than one radiated photon, and a small fraction of q$\bar{\mathrm{q}}$ events.

3.2 Selection of $\ell\ell\gamma$ Final States

Events containing two lepton candidates of the same flavour and at least one identified photon are considered as candidate events for the single production of excited leptons. In addition, events with two leptons of different flavours and at least one photon are considered as excited tau candidates. If more than one photon is identified in the event, the most energetic photon is chosen and the other photon is ignored. Events selected as candidates for the pair production of excited leptons are also considered as single production candidates.

To reduce the background from two-photon events the quantity R_{vis} must be greater than 0.8 for eeγ and $\mu\mu\gamma$ candidates, and greater than 0.4 for $\tau\tau\gamma$ candidates. The R_{vis} distributions of each type of candidate event are shown in Figure 1(d-f) for data from all the centre-of-mass energies combined.

The dominant e$^+$e$^-$ background in the eeγ final state is reduced by requiring that the angle between the most energetic electron and photon ($\theta_{\mathrm{e}\gamma}$) be greater than 90^0. The $\cos\theta_{\mathrm{e}\gamma}$ distribution obtained using data from all centre-of-mass energies combined is shown in Figure 2(a).

Background from both e$^+$e$^-$ and $\mu^+\mu^-$ events in the $\tau\tau\gamma$ sample is reduced by requiring the total energy deposited in the electromagnetic calorimeter to be between 20% and 80% of the centre-of-mass energy. Finally, the polar angle of the missing momentum vector for the particles considered in the $\tau\tau\gamma$ final state must lie within $|\cos\theta_{\mathrm{miss}}| < 0.9$. This requirement reduces the contamination from q$\bar{\mathrm{q}}$ events. Figures 2(b,c) show both the total electromagnetic energy and $|\cos\theta_{\mathrm{miss}}|$ distributions of $\tau\tau\gamma$ events before applying each cut.

After this selection, the remaining background in the eeγ and $\mu\mu\gamma$ samples consists almost entirely of e$^+$e$^-$ and $\mu^+\mu^-$ events with an additional photon. The background in the $\tau\tau\gamma$ sample consists mostly of $\tau^+\tau^-$ events with one radiated photon and a small fraction of radiative e$^+$e$^-$, $\mu^+\mu^-$ and q$\bar{\mathrm{q}}$ events.

3.3 Selection of eγ Final State

A separate selection for events with one electron and one photon was developed to increase the efficiency of the search for singly produced excited electrons where one electron travels in the forward region outside the detector acceptance.

Candidate events are required to contain at least one photon and at least one electron candidate. Additional jets, if present, are ignored. Since the eeγ and eγ final states are combined to calculate a limit on the single production of excited electrons, it is important to ensure that events are not double-counted. All events that are selected by the set of general requirements discussed at the beginning of Section 3, but that fail the eeγ selection are considered as possible eγ candidates.

To reduce the two-photon background, the quantity R_{vis} must satisfy $R_{\mathrm{vis}} > 0.4$. The angle between the electron and photon ($\theta_{e\gamma}$) is also required to be greater than 90^0. Further reduction of the dominant e^+e^- background is achieved by requiring that the measured polar angle of the photon satisfies $|\cos\theta_\gamma| < 0.8$ and by rejecting events where the photon is identified as a conversion.

Figures 2(d-f) show the R_{vis}, $\cos\theta_{e\gamma}$ and $|\cos\theta_\gamma|$ distributions of eγ events obtained using the entire data set with cuts applied in the order described above. The irreducible background consists almost entirely of e^+e^- events with one radiated photon.

3.4 Kinematic Fits

The existence of excited leptons would reveal itself as an excess in the total number of observed events, appearing as a peak in the reconstructed $\ell\gamma$ invariant mass distributions. Kinematic fits are used to improve the reconstructed mass resolution of the selected events and also further reduce the background thereby increasing the sensitivity of the analysis to excited leptons.

The kinematic variables used as input to the fit are the energy and direction (E, θ, ϕ) of each identified jet in an event. The energy of tau candidates is left as a free parameter and the direction is taken to be the jet axis. A kinematic fit also requires as input the error on each measured variable. Estimates of the uncertainties on the energy and direction for the different types of leptons and for photons are obtained from studies of di-lepton events in data recorded at centre-of-mass energies near and greater than the Z^0 mass. The error estimates are parameterised as functions of the jet energy and polar angle. The uncertainty on the jet energy is typically 2 GeV for electrons and photons, and about 5 GeV for muon candidates. The uncertainty on the jet polar angle is about 2 mrad for electrons and muons, 4 mrad for photons, and 7 mrad for tau candidates. Finally, the azimuthal angle of electron, muon, photon and tau candidates is typically known to 0.4 mrad, 0.4 mrad, 3.5 mrad and 7 mrad respectively.

The kinematic fit enforces conservation of energy and momentum while taking into account the beam energy spread as measured by the LEP energy working group [8]. This last constraint is necessary since the expected mass resolution for excited leptons is of the same order as the centre-of-mass energy spread, which is measured to be approximately 250 MeV.

Slightly different kinematic fits are applied for single and pair production candidate events. In addition to energy and momentum conservation, the kinematic fits for pair produced excited lepton candidates also require the invariant masses of the two lepton-photon pairs in the event to be equal. There are two possible lepton-photon pairings in each event, and for each pairing an additional fit is performed assuming the presence of an undetected initial state radiation photon along the beam axis. Thus for each pair production candidate, four kinematic fits are performed. Similarly, two kinematic fits are applied to singly produced excited lepton candidate events. In the first case, only the two leptons and one photon are included in the fit. In the second case, the fit is performed assuming the presence of an initial state radiation photon along the beam axis. Finally, a single kinematic fit is performed for eγ events. The fit assumes the presence of an undetected electron along the beam axis.

For a given final state, events are rejected if every kinematic fit attempted has a probability less than 0.001. When more than one successful kinematic fit is obtained for an event, the fit performed without the presence of an initial state radiation photon is chosen if the fit probability is

greater than 0.001. For pair production candidates where two fits without initial state radiation are performed, the lepton-photon pairing corresponding to the fit with the highest probability in excess of 0.001 is chosen. Otherwise, results from the fit with an initial state radiation photon are retained where, for pair production candidates, the lepton-photon pairing corresponding to the fit with the highest probability is chosen. This requirement on the kinematic fit probabilities reduces the number of selected events by more than 70% for $\ell\ell\gamma\gamma$ final states and by about 10% for final states compatible with the single production of an excited lepton.

Results from the chosen kinematic fit for each event are used to calculate $\ell\gamma$ invariant masses. Using the procedure outlined above, the correct lepton-photon pairing for pair produced excited leptons is chosen more than 98% of the time as determined using simulated signal events. For $\ell\ell\gamma$ events, two lepton-photon combinations are possible, both of which are included in the analysis. Mass resolutions of approximately 0.2-0.4 GeV for excited electrons and muons and 0.7-2.0 GeV for excited taus are obtained using results from the kinematic fits. The natural decay width of excited leptons for couplings not excluded by previous searches is constrained to be much smaller than these mass resolutions and is thus neglected. Figure 3 shows the invariant mass distributions of selected $\ell\ell\gamma$ and eγ events. There are two entries per $\ell\ell\gamma$ event, corresponding to the two possible lepton-photon pairings. These distributions are obtained by combining data from all the centre-of-mass energies considered. In both single and pair production event samples, no mass peaks are observed in the data.

4 Results

The numbers of events observed in the data and the corresponding numbers of background events expected from Standard Model processes are shown in Table 2. Selected candidate events for the pair production of excited leptons are listed in Table 3. Typical selection efficiencies for the pair production of excited leptons vary from about 35% to 55%. The efficiency for the single production of excited muons is 70% and approximately constant over the entire kinematically allowed range of masses. Near the kinematic limit for the single production of excited taus, the efficiency rapidly drops from 53% down to approximately 20% since the recoiling tau has low energy and thus often fails the initial set of selection criteria. For singly produced excited electrons, the efficiencies of the eeγ and eγ selections depend strongly on the mixture of s-channel and t-channel components. The sum of the eeγ and eγ efficiencies is typically between 50% and 70%. The evaluation of the systematic uncertainties on the selection efficiencies and background estimates is discussed in the following section. No excess of data indicating the existence of excited leptons is found in either the single or pair production search.

4.1 Systematic Uncertainties

The following sources of systematic uncertainties on the signal efficiencies and background estimates were investigated. These are described in order of importance.

Uncertainties in the modelling of initial state photon radiation (ISR) in di-lepton events affect the background estimates. They are assessed by comparing background expectations from the KORALZ and KK2F event generators for the processes $e^+e^- \to \mu^+\mu^-$ and $e^+e^- \to \tau^+\tau^-$. The Monte Carlo program KK2F, used in this analysis to estimate the background contributions from $\mu^+\mu^-$ and $\tau^+\tau^-$ events, has the most complete description of initial state radiation including second-order subleading corrections and the exact matrix elements for two hard photons [29]. The relative variations in background expectations between the two Monte Carlo generators are assigned as systematic uncertainties representing the effect of missing higher orders. These are found to be 11% for final states compatible with the single production of excited muons and taus, and 7% for $\mu\mu\gamma\gamma$ and $\tau\tau\gamma\gamma$ events. The BHWIDE and TEEGG event generators, used to

	$ee\gamma$	$e\gamma$	$\mu\mu\gamma$	$\tau\tau\gamma$	$ee\gamma\gamma$	$\mu\mu\gamma\gamma$	$\tau\tau\gamma\gamma$
Data	1172	1123	212	248	3	3	7
Background	1283	1229	239	260	4.0	2.0	8.0
Background statistical errors	11	14	2	2	0.6	0.2	0.6
Background systematic errors	161	159	28	40	1.2	0.7	6.3

Sources of background systematic errors							
ISR modelling	141	135	26	29	0.3	0.1	0.6
Error estimate of fit variables	68	57	10	24	1.1	0.6	6.2
Jet classification	36	27	3	12	0.2	0.1	0.5
Energy and angular resolution	9	16	2	2	0.0	0.3	0.6
Modelling of selection variables	6	54	2	8	0.3	0.1	0.3

Table 2: Total numbers of selected events in the data and expected numbers of background events for the different final states considered. Statistical and total systematic uncertainties on the background estimates are also shown. Contributions to the total systematic errors on the background expectations are listed in the lower part of the table.

$ee\gamma\gamma$		$\mu\mu\gamma\gamma$		$\tau\tau\gamma\gamma$	
$\sqrt{s}$ (GeV)	$m_{e\gamma}$ (GeV)	$\sqrt{s}$ (GeV)	$m_{\mu\gamma}$ (GeV)	$\sqrt{s}$ (GeV)	$m_{\tau\gamma}$ (GeV)
188.7	39.3	188.7	44.5	188.6	70.9
199.6	80.1	205.1	28.0	189.0	52.7
201.6	92.7	206.2	34.0	199.6	30.1
				199.7	76.2
				204.7	39.1
				204.8	38.6
				205.1	88.6

Table 3: List of selected candidate events for the pair production of excited leptons. For each candidate, the centre-of-mass energy and reconstructed invariant mass obtained after performing the kinematic fits are listed.

simulate the background from radiative e^+e^- events, have a precision for radiative corrections similar to the KORALZ program. The background estimates for events expected from the production of excited electrons are thus assigned an uncertainty of 7% for the $ee\gamma\gamma$ final state and 11% for both $ee\gamma$ and $e\gamma$ events. This uncertainty is significantly larger than the error for inclusive electron pair production cited in [30].

For the purpose of calculating limits on the product of the cross-section and the branching fraction, it is necessary to be able to calculate the efficiency and mass resolution of signal events at arbitrary excited lepton masses and centre-of-mass energies. For each final state, the selection efficiencies and mass resolutions are parameterised as a function of the excited lepton mass scaled by the centre-of-mass energy ($m_{\ell*}/\sqrt{s}$). The systematic uncertainties associated with the interpolation of efficiencies and mass resolutions were estimated by calculating the root-mean-square spread between simulated signal event samples and the parameterisation functions.

Uncertainties on the fit variable error estimates are evaluated by varying the errors on each variable independently. The errors are varied by an amount representing one standard deviation as calculated from the uncertainties on the energy and angular parameterisation. Background estimates for final states containing two leptons and two photons are particularly sensitive to

changes in the errors due to the additional constraint in the kinematic fit requiring events to have equal reconstructed lepton-photon invariant masses. Also, the smaller sample of tau pair events used to parameterise the errors on the tau direction results in larger statistical uncertainties on the error parameterisation which in turn dictate the larger variations used to estimate the systematic error contributions.

The jet classification into leptons or photons contributes to the overall systematic uncertainty through the modelling of the lepton and photon identification efficiencies. Using di-lepton and di-photon events recorded at centre-of-mass energies equal to and greater than the Z^0 mass, the systematic uncertainty associated with each set of lepton and photon requirements was evaluated by comparing the identification efficiencies obtained from data and simulated events. Relative errors of 1% for electron and muon, and 2% for the tau and photon classifications are assigned. Systematic uncertainties associated with each final state were determined by adding linearly contributions from identical jet classifications and adding in quadrature contributions from different types of leptons and photons. The resulting uncertainties on the signal efficiencies, shown in Table 4, are fully correlated with the corresponding errors on the background estimates presented in Table 2.

The systematic uncertainty associated with the energy scale, energy resolution and angular resolution of the leptons and photons was evaluated by modifying each parameter independently in Monte Carlo simulated events. Comparisons between data and simulated distributions of di-lepton events recorded at different centre-of-mass energies were used to determine the size of these variations. The energy (momentum) of electron and photon (muon) candidates was shifted by 0.3%. The energy and angular resolutions of jets were smeared by the maximum values for which simulated events were compatible with the distribution of data within one standard deviation. Variations in the energy scale result in negligible changes in efficiencies and background. Contributions to the systematic uncertainty of each final state from individual changes in the energy and angular resolution are added in quadrature.

The systematic uncertainty due to Monte Carlo modelling of the event selection variables was estimated by varying each selection cut independently and measuring the corresponding changes in the overall signal efficiencies and background estimates. The difference between the mean value of the data and background expectation for each selection variable determined the range of variation of each cut. Systematic uncertainties varying between 0.5% and 6.3% are assigned to the different background estimates. Contributions to the systematic error on the signal efficiencies are shown in Table 4.

Lastly, the uncertainty on the integrated luminosity measurements (0.2%) is considerably smaller than the systematic effects already described and is therefore neglected.

Summaries of the systematic effects on the background expectations and signal efficiencies are presented in Tables 2 and 4, respectively. These systematic uncertainties are included in the calculation of limits as described in the following section.

4.2 Limit Calculations

Limits on the product of the cross-section and the electromagnetic branching fraction of excited leptons are obtained from both pair and single production searches. The numbers of data and expected background events at each centre-of-mass energy are binned as a function of the reconstructed invariant mass. For selected $\ell\ell\gamma$ candidates, both possible $\ell\gamma$ invariant masses are used. Due to the excellent mass resolution, the double-counting of $\ell\ell\gamma$ events does not affect the limits calculated. Each mass bin at a given centre-of-mass energy is treated as an independent counting experiment.

For the purpose of calculating limits, the signal invariant mass is assumed to be well described by a Gaussian distribution centred at the test mass value and with a width equal to the expected

Source	Uncertainty (%)						
	$ee\gamma$	$e\gamma$	$\mu\mu\gamma$	$\tau\tau\gamma$	$ee\gamma\gamma$	$\mu\mu\gamma\gamma$	$\tau\tau\gamma\gamma$
Resolution interpolation	18.6	12.5	20.7	7.1	23.5	18.1	12.9
Efficiency interpolation	8.6	3.0	2.3	5.3	4.5	3.4	4.4
Error estimate of fit variables	5.0	5.0	3.0	5.0	3.0	2.0	6.0
Jet classification	2.8	2.2	1.4	4.5	4.5	4.5	5.7
Energy and angular resolution	0.9	1.1	0.8	1.1	1.8	0.6	0.9
Modelling of selection variables	0.0	1.5	0.1	1.6	0.4	0.4	0.8
Total	21.3	14.1	21.1	11.3	24.6	19.1	16.0

Table 4: Relative systematic uncertainties on the signal efficiencies for each final state considered.

mass resolution. The validity of this assumption is verified with Monte Carlo simulation of signal events at different masses and centre-of-mass energies. Efficiency corrections due to non-Gaussian tails in the invariant mass distributions are applied to the signal expectation. These correction factors, signal efficiencies and mass resolutions are all parameterised as a function of the excited lepton mass scaled by the centre-of-mass energy, $m_{\ell*}/\sqrt{s}$. The efficiency correction factors are constant over the entire kinematically allowed range and vary from approximately 0.7 to 0.85 depending on the event final state. Efficiencies and mass resolutions are well-described by polynomial functions of various degrees. The efficiencies for the single production of excited leptons are calculated with the production and decay angular distributions corresponding to $f = f'$. The assignment $f = f'$ particularly affects the relative fraction of excited electron events in the $e\gamma$ and $ee\gamma$ selections.

For a given test mass, the Gaussian distributions describing the invariant mass of signal events at each centre-of-mass energy considered are normalised to the expected excited lepton cross-section at the highest centre-of-mass energy, thereby taking into account the energy dependence of the cross-section. A likelihood ratio method [31] is used to compute the 95% confidence level upper limit on the number of signal events produced in the entire data set (N_{95}). Systematic uncertainties on the signal efficiency and background expectation are incorporated by fluctuating, over many iterations, the background expectation and signal efficiency according to their respective systematic uncertainties. The final limits are determined from the average of all the N_{95} values obtained at each iteration. Systematic errors on the background estimates are treated as being fully correlated. The systematic uncertainties on the signal efficiencies due to the jet classification are also fully correlated with the corresponding errors on the background estimates and are treated as such in the limit calculations.

Limits on the product of the cross-section and the branching fraction are scaled to $\sqrt{s} = 208.3$ GeV assuming the cross-section evolution as a function of centre-of-mass energy expected for excited leptons. The upper limits on the single production of excited muons and tau leptons do not depend on the coupling assignment of f and f'. The excited electron selection efficiencies, however, depend on the relative magnitude of the s-channel and t-channel diagrams. For comparison with previously published results, the limits on excited electrons presented here assume $f = f'$. Figures 4(a,b) show the 95% confidence level upper limits on the product of the cross-section at $\sqrt{s} = 208.3$ GeV and the branching fraction obtained from the search for singly and pair produced excited leptons.

The theoretical calculation [5] of the product of the pair production cross-section at $\sqrt{s} = 208.3$ GeV and the branching fraction squared is overlaid on Figure 4(b). As part of this calculation, the electromagnetic branching fraction is calculated assuming $f = f'$. The 95% confidence level lower mass limits on excited leptons correspond to the mass at which the cross-section times branching fraction limit curves cross the theoretical expectation. Lower mass limits

of $m_{e^*} > 103.2$ GeV, $m_{\mu^*} > 103.2$ GeV and $m_{\tau^*} > 103.2$ GeV are obtained. Although systematic errors are incorporated into the limit calculations, an additional uncertainty on the mass limits arises from the finite width of the centre-of-mass energy bins considered. The 0.5 GeV centre-of-mass energy bin width near the kinematic limit corresponds to an uncertainty of 0.1 GeV on the mass limits.

Limits on the product of the cross-section and the electromagnetic branching fraction of singly produced excited leptons are used to constrain parameters of the model introduced in Section 1. Since the cross-section for the single production of excited leptons is proportional to $(f/\Lambda)^2$, limits on the ratio of the coupling to the compositeness scale as a function of excited lepton mass are calculated using

$$\left[\frac{(f/\Lambda)}{(1 \text{ TeV}^{-1})}\right]_{95\%\text{CL}} = \sqrt{\frac{N_{95}}{N_{exp}}} \quad ,$$

where N_{exp} is the number of expected signal events assuming $f/\Lambda = 1$ TeV^{-1}. Figure 4(c) shows these limits for each type of excited lepton. The f/Λ limit for excited electrons is approximately an order of magnitude better than for muons and taus due to the enhancement of the cross-section coming from the t-channel contribution.

5   Conclusion

A search for electromagnetically decaying charged excited leptons was performed using 684.4 pb^{-1} of data collected by the OPAL detector at $\sqrt{s} = 183$-209 GeV. No evidence was found for the existence of excited leptons. Upper limits on the product of the cross-section and the branching fraction were calculated. From pair production searches, 95% confidence level lower limits on the mass of excited leptons are determined to be $m_{\ell^*} > 103.2$ GeV for $\ell = e, \mu, \tau$. From the results of the search for singly produced excited leptons, limits were calculated on the ratio of the coupling constant to the compositeness scale (f/Λ) as a function of excited lepton mass. The results are currently the most stringent constraints on the existence of excited leptons and therefore represent a significant improvement on limits previously published [2–4].

References

[1] F.E. Low, Phys. Rev. Lett. **14** (1965) 238.

[2] OPAL Collaboration, G. Abbiendi *et al.*, Eur. Phys. J. **C14** (2000) 73;
OPAL Collaboration, K. Ackerstaff *et al.*, Eur. Phys. J. **C1** (1998) 45;
OPAL Collaboration, K. Ackerstaff *et al.*, Phys. Lett. **B391** (1997) 197;
OPAL Collaboration, G. Alexander *et al.*, Phys. Lett. **B386** (1996) 463;
OPAL Collaboration, M.Z. Akrawy *et al.*, Phys. Lett. **B244** (1990) 135.

[3] L3 Collaboration, M. Acciarri *et al.*, Phys. Lett. **B502** (2001) 37;
DELPHI Collaboration, P. Abreu *et al.*, Eur. Phys. J. **C8** (1999) 41;
ALEPH Collaboration, R. Barate *et al.*, Eur. Phys. J. **C4** (1998) 571.

[4] H1 Collaboration, C. Adloff *et al.*, Phys. Lett. **B525** (2002) 9;
H1 Collaboration, C. Adloff *et al.*, Eur. Phys. J. **C17** (2000) 567;
ZEUS Collaboration, S. Chekanov, *et al.*, Submitted to Phys. Lett. **B** [hep-ex/0109018];
ZEUS Collaboration, J. Breitweg *et al.*, Z. Phys. **C76** (1997) 631;
ZEUS Collaboration, M. Derrick *et al.*, Z. Phys. **C65** (1995) 627.

[5] F. Boudjema, A. Djouadi and J.L. Kneur, Z. Phys. **C57** (1993) 425.

[6] K. Hagiwara, D. Zeppenfeld and S. Komamiya, Z. Phys. **C29** (1985) 115.

[7] OPAL Collaboration, S. Anderson *et al.*, Nucl. Instr. Meth. **A403** (1998) 326;
B.E. Anderson *et al.*, IEEE Trans. Nucl. Sci. **41** (1994) 845;
OPAL Collaboration, K. Ahmet *et al.*, Nucl. Instr. Meth. **A305** (1991) 275.

[8] LEP Energy Working Group, A. Blondel *et al.*, Eur. Phys. J. **C11** (1999) 573.

[9] R. Tafirout and G. Azuelos, Comp. Phys. Comm. **126** (2000) 244.

[10] A. Djouadi, Z. Phys. **C63** (1994) 317.

[11] S. Jadach, W. Płaczek and B.F.L. Ward, Phys. Lett. **B390** (1997) 298.

[12] D. Karlen, Nucl. Phys. **B289** (1987) 23.

[13] S. Jadach, B.F.L. Ward and Z. Wąs, Comp. Phys. Comm. **79** (1994) 503.

[14] S. Jadach, B.F.L. Ward and Z. Wąs, Comp. Phys. Comm. **130** (2000) 260;
S. Jadach, B.F. Ward and Z. Wąs, Phys. Lett. **B449** (1999) 97.

[15] T. Sjöstrand, Comp. Phys. Comm. **82** (1994) 74.

[16] S. Jadach, W. Płaczek, M. Skrzypek, B.F.L. Ward and Z. Wąs, Comp. Phys. Comm. **119** (1999) 272.

[17] J. Fujimoto *et al.*, Comp. Phys. Comm. **100** (1996) 128.

[18] F.A. Berends, R. Kleiss, Nucl. Phys. **B186** (1981) 22.

[19] R. Bhattacharya, J. Smith and G. Grammer, Phys. Rev. **D15** (1977) 3267;
J. Smith, J.A.M. Vermaseren and G. Grammer, Phys. Rev. **D15** (1977) 3280.

[20] R. Engel and J. Ranft, Phys. Rev. **D54** (1996) 4244.

[21] G. Marchesini *et al.*, Comp. Phys. Comm. **67** (1992) 465.

[22] J. Allison *et al.*, Nucl. Instr. Meth. **A317** (1992) 47.

[23] OPAL Collaboration, G. Alexander *et al.*., Z. Phys. **C72** (1996) 191.

[24] OPAL Collaboration, G. Alexander *et al.*, Z. Phys. **C52** (1991) 175.

[25] OPAL Collaboration, R. Akers *et al.*, Z. Phys. **C63** (1994) 197.

[26] OPAL Collaboration, G. Abbiendi *et al.*, Eur. Phys. J. **C16** (2000) 41;
OPAL Collaboration, G. Abbiendi *et al.*, Eur. Phys. J. **C8** (1999) 217;
OPAL Collaboration, G. Alexander *et al.*, Z. Phys. **C70** (1996) 357.

[27] OPAL Collaboration, K. Ackerstaff *et al.*, Phys. Lett. **B389** (1996) 416.

[28] OPAL Collaboration, K. Ackerstaff *et al.*, Eur. Phys. J. **C2** (1998) 213.

[29] S. Jadach, B. F. L. Ward and Z. Wąs, Phys. Rev. **D63** (2001) 113009.

[30] S. Jadach, W. Płaczek and B.F.L. Ward in "Two-Fermion Production in Electron-Positron Collisions", edited by M. Kobel and Z. Wąs, CERN-2000-009-D [hep-ph/0007180].

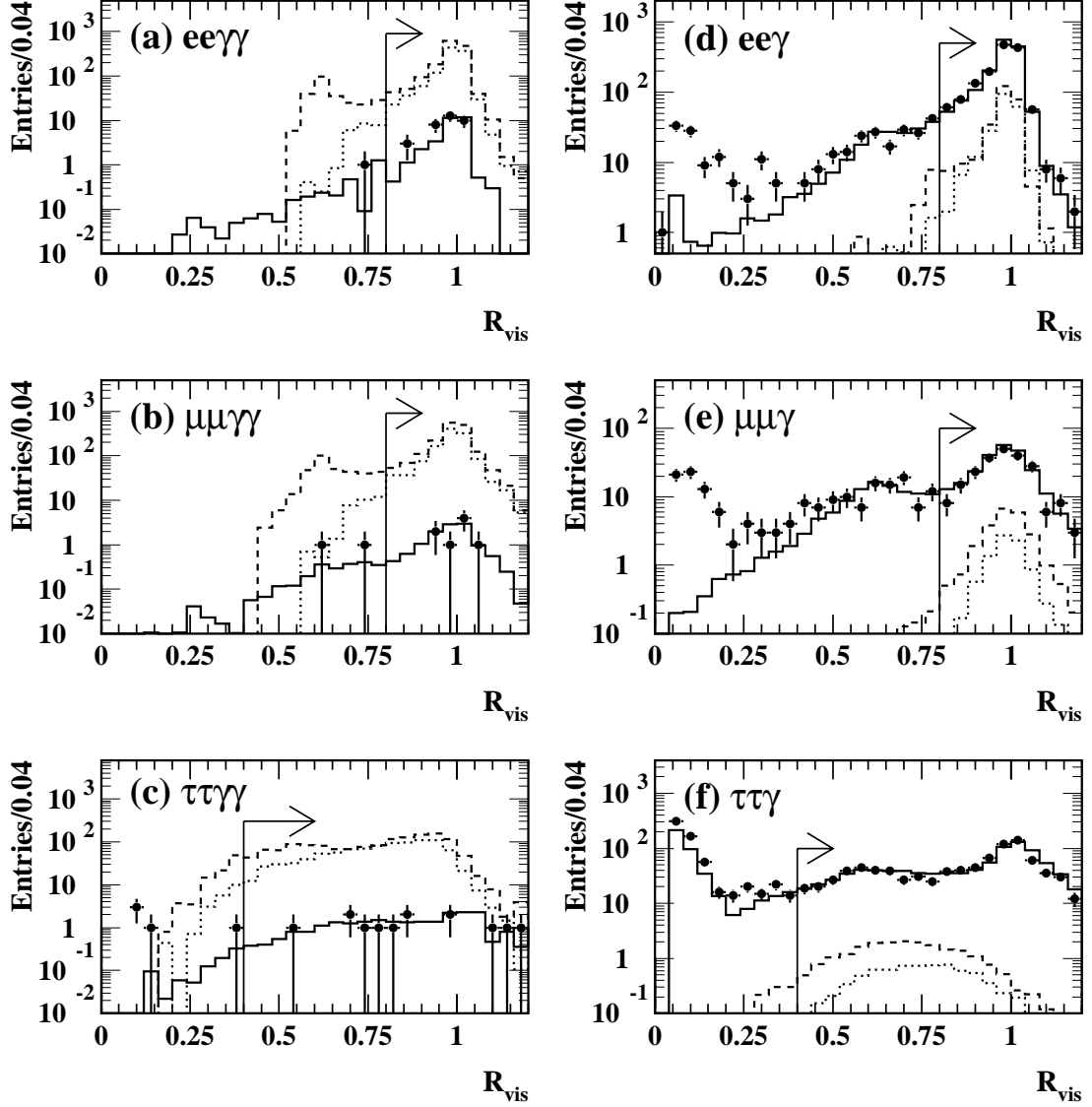[31] T. Junk, Nucl. Instr. Meth. **A434** (1999) 435.

OPAL

Figure 1: Distributions of the sum of the energies of the two leptons and one or two photons divided by the centre-of-mass energy for pair (a-c) and single (d-f) production candidate events after the preselection. The points represent the combined data from all centre-of-mass energies considered while the solid lines are the total expected background from Standard Model processes. The dashed lines represent an example of $\ell^*\ell^*$ (a-c) and ℓ^*(d-f) signal events with arbitrarily chosen masses of 40 GeV and 90 GeV respectively. The dotted lines show the expected distributions for pair and singly produced excited leptons with masses of 90 GeV and 180 GeV, respectively. Distributions of excited lepton signal events are normalised to a ratio of the coupling constant to the compositeness scale of 1 TeV^{-1}. The arrows indicate the accepted regions. The background modelling for low values of R_{vis} is discussed in Section 3.1.
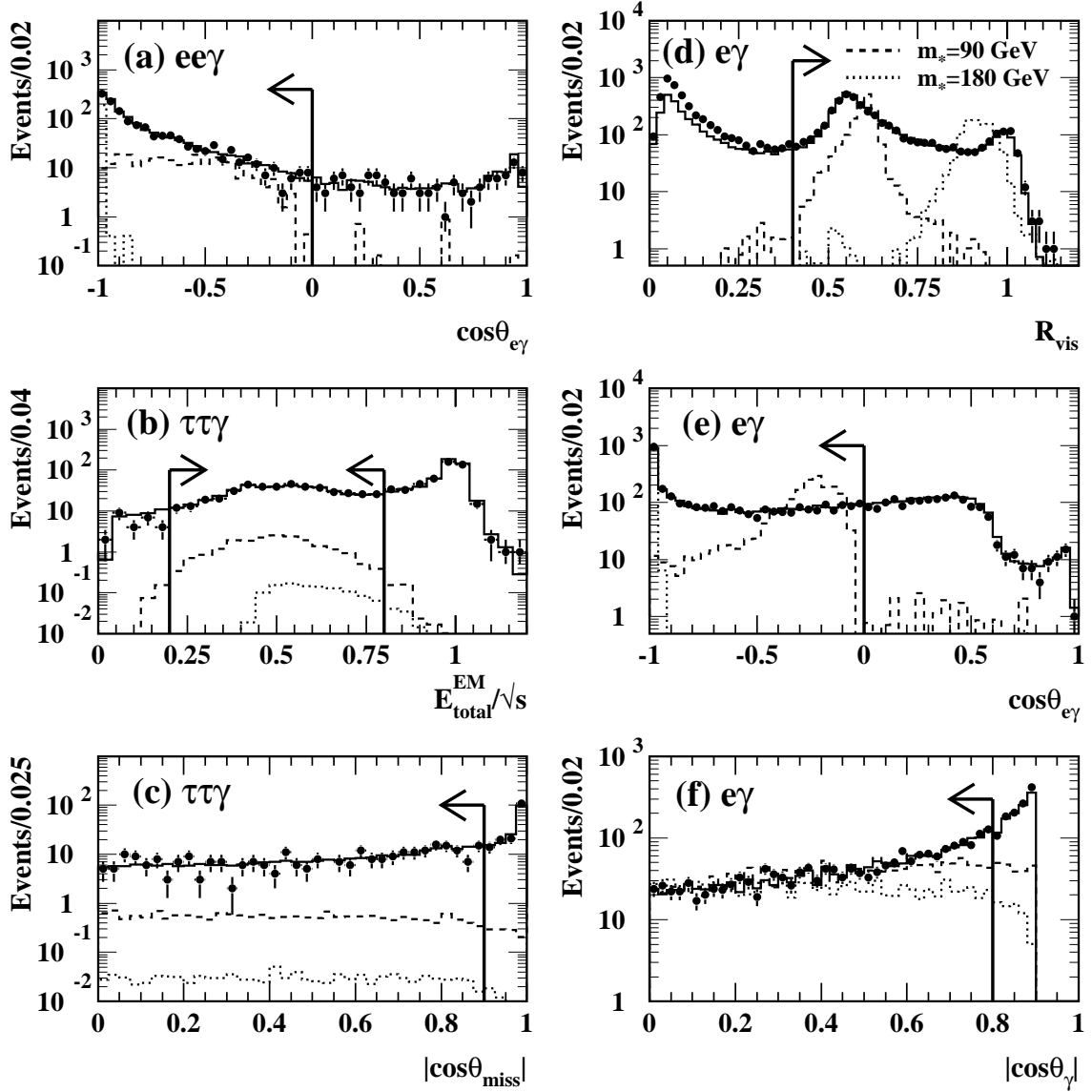
15

OPAL

Figure 2: Distributions of selection variables for different final states: (a) cosine of the angle between the most energetic electron and the photon in eeγ events, (b) total energy deposited in the electromagnetic calorimeter scaled by the centre-of-mass energy for $\tau\tau\gamma$ events, (c) absolute value of the cosine of the missing momentum vector polar angle for $\tau\tau\gamma$ events, (d) sum of the energy of the electron and photon divided by the centre-of-mass energy for eγ events, (e) cosine of the angle between the electron and photon for eγ events and (f) absolute value of the cosine of the photon polar angle in eγ events. All selection cuts have been applied, in the same order as described in the text, up to that on the variable plotted. The dashed and dotted lines represent examples of excited lepton signal events with arbitrarily chosen masses of 90 GeV and 180 GeV, respectively, and branching fraction calculated assuming a ratio of the coupling constant to the compositeness scale of 1 TeV^{-1}.
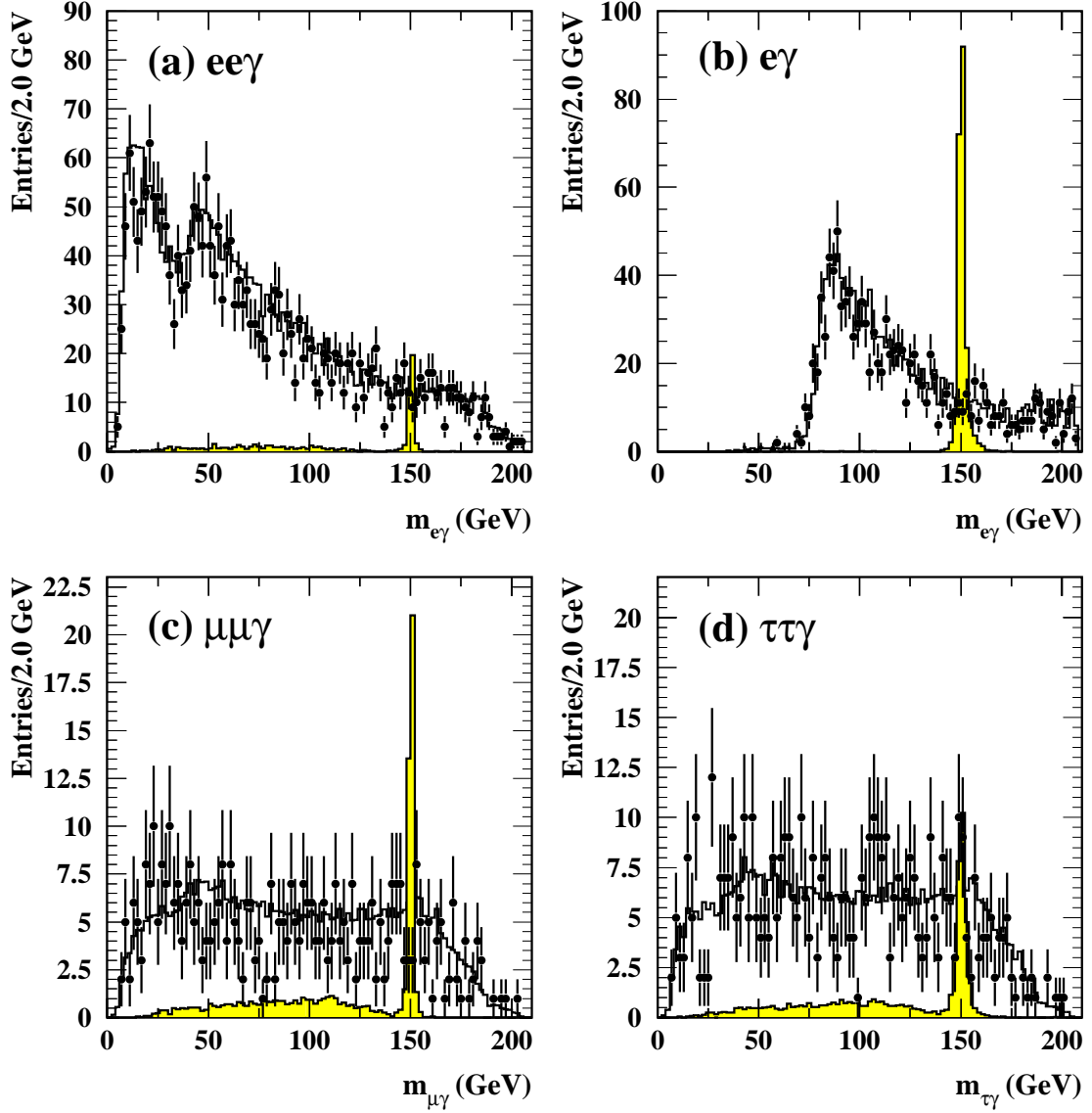
16

OPAL

Figure 3: Reconstructed invariant mass distributions for (a) $ee\gamma$, (b) $e\gamma$, (c) $\mu\mu\gamma$ and (d) $\tau\tau\gamma$ candidates after all cuts are applied. The points are data and the solid lines represent the total expected background from Standard Model processes. The shaded histograms represent excited lepton signal events with an arbitrarily chosen mass of 150 GeV and normalised to a ratio of the coupling constant to the compositeness scale of 0.4 TeV^{-1} (a,b) and 2 TeV^{-1} (c,d). There are two entries per event in (a,c,d) corresponding to the two possible $\ell\gamma$ pairings.
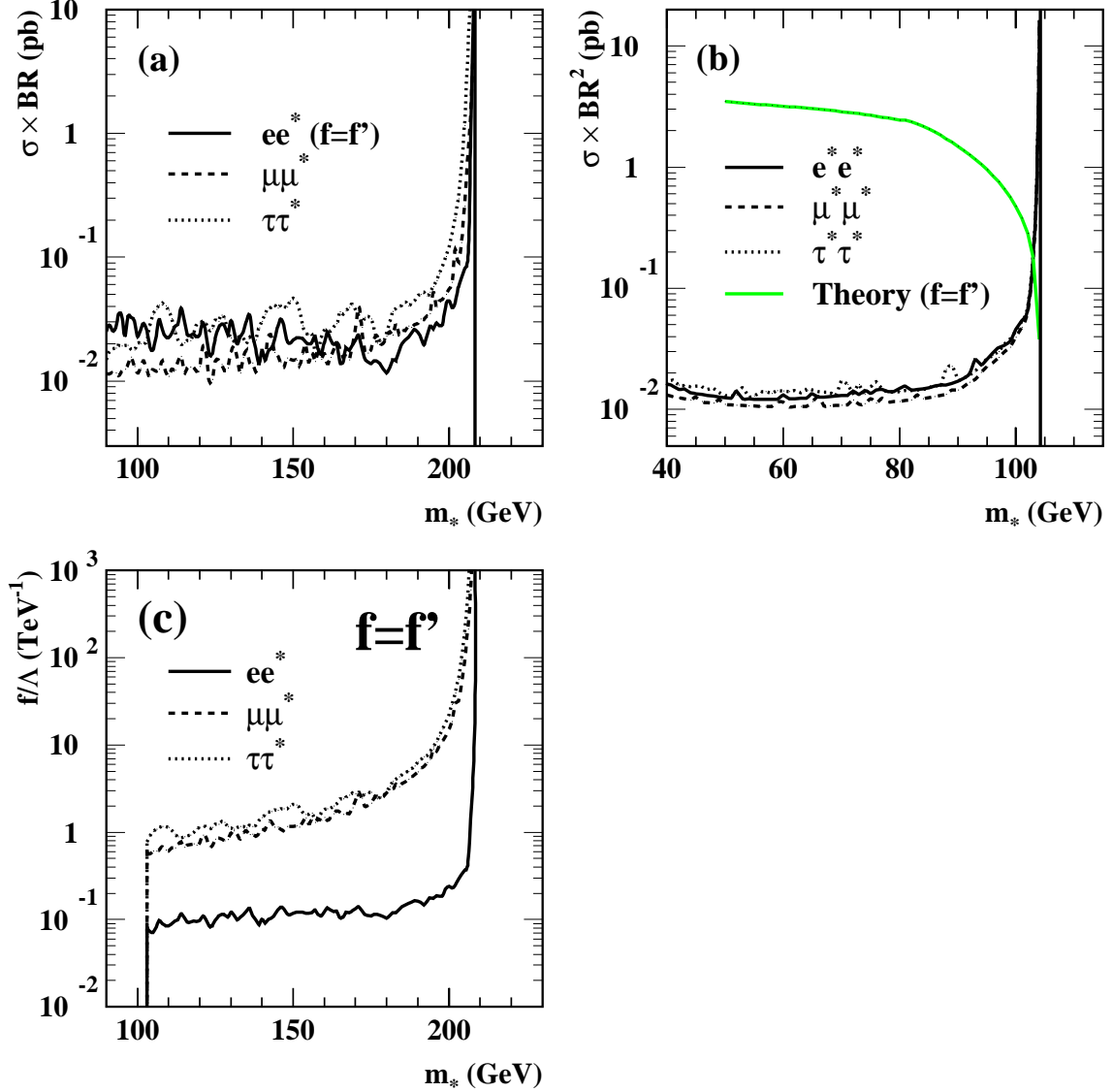
OPAL

Figure 4: The 95% confidence level upper limits on the product of the cross-section at $\sqrt{s} = 208.3$ GeV and the branching fraction for (a) single and (b) pair production of excited leptons as a function of mass (m_*). The limit obtained for the single production of excited electrons is calculated assuming $f = f'$. The regions above the curves are excluded. The product of the theoretical cross-section and the branching fraction squared assuming $f = f'$ is also shown in (b). The 95% confidence level upper limits on the ratio of the excited lepton coupling constant to the compositeness scale, f/Λ, as a function of the excited lepton mass and assuming $f = f'$ are shown in (c). The regions above the curves are excluded by single production searches while pair production searches exclude masses below 103.2 GeV for excited electrons, muons and taus.